Measurements of the Bottom Loss Magnitude and Phase from 5 to 50 kHz and 10 to 77 degrees grazing at the Experimental Validation of Acoustic modeling techniques (EVA) Sea Test

Marcia J. Isakson, Nicholas P. Chotiros
and James N. Piper
Applied Research Laboratories
The University of Texas at Austin
Austin, Texas 78713
Email: misakson@arlut.utexas.edu

Mario Zampolli
NATO Underseas Research Centre
La Spezia, Italy

***Abstract*—The value of the specular bottom loss is an important parameter for modeling the propagation of acoustic waves in littoral areas. In shallow waters, even short range propagation can have many interactions with the ocean bottom. Bottom loss is affected by many envorinmental parameters including the reflection coefficient, which is dependent on the sediment type, and scattering from the water/sediment interface. The phase and magnitude of the reflection coefficient from 5 to 50 kHz and 10 to 77 degrees grazing from a rough sand/water interface were taken as part of the Experimental Validation of Acoustic modeling techniques (EVA). The experiment was conducted off the coast of Isola dElba in October 2006. The measurements were corrected for beam pattern and rough interface scattering effects and compared with two current models describing acoustic interaction with ocean sediments, the elastic model and the Effective Density Fluid Model (EDFM) [1]. Both models are corrected for spherical wave effects using the experimental geometry.**

I. Experimental Set-Up

The experiment was conducted in Biodola Bay off the coast of Isola dElba, Italy on October 2006 as part of the Experimental Validation of Acoustic modeling techniques (EVA). Hydrophones to measure bottom loss were deployed from the Coastal Research Vessel (CRV) Leonardo. Four receiving hydrophones and one source transducer were deployed from the ship so that the grazing angle range from 10 77 degrees could be measured. (See Figure 1.) The receivers were placed at nominal ranges of 1.2 m, 2.8m, 7.5m and 20m from the source. The exact ranges were measured as part of the experiment. The two closest receivers and the source were deployed from the the starboard side while the remaining receivers were deployed from the port side. The source (open circle in Figure 1) was raised and lowered to cover the angle range. All five hydrophones were weighted with dive shot which was found to be acoustically dark in this frequency range.

The large frequency range (5 50 kHz) was accommodated by using a broadband chirp pulse. The pulse length was 1 ms. A 50 dB dynamic range for the experimental set-up was measured over the frequency range. A custom pulse was designed to reduce the dynamic range by increasing the number of cycles for off resonance frequencies. A dynamic range of 20 dB was therefore achieved without amplitude shading for the frequency range of 5 to 50 kHz. (See Figure 2.)

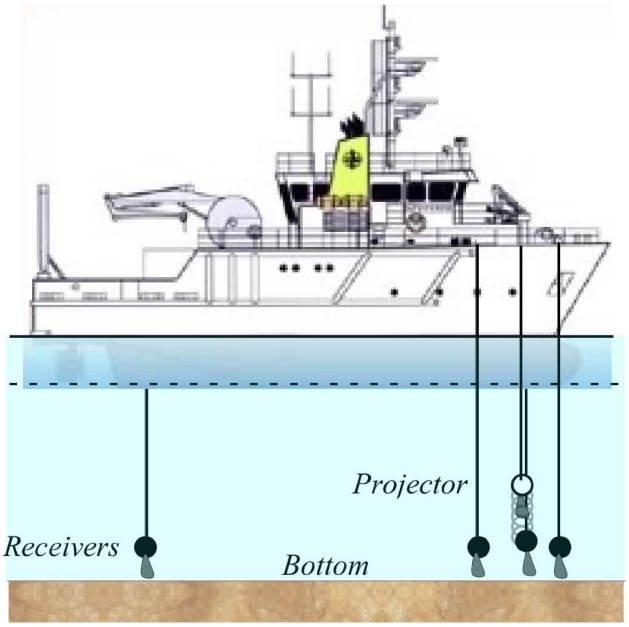

Fig. 1. Experimental Set-Up for Bottom Loss Measurement

Bottom loss measurements were taken in 12 m of water in Biodola Bay, Isola d'Elba. The site was composed of medium sand and was free of sea grass as seen visually on site and by satellite photo. There was no apparent ripple structure on the ocean floor. Measurements of the interface roughness was taken daily using a laser profiler system using the set-up described in [2]. From these measurements, the interface

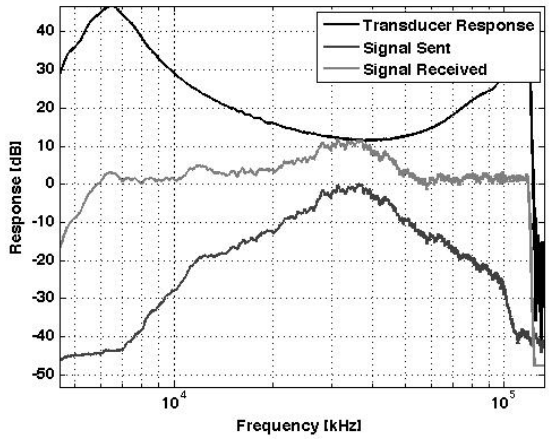

(a) Frequency Response

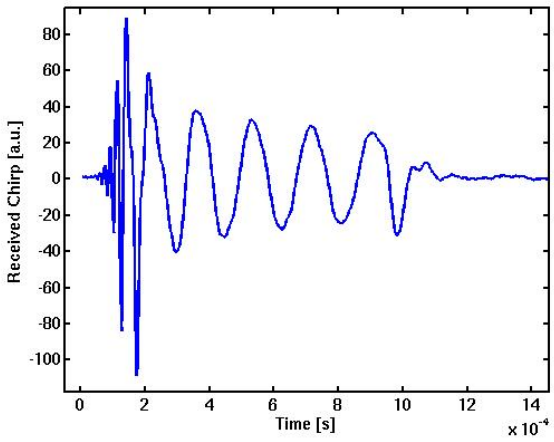

(b) Signal Received

Fig. 2. In Figure 2(a) is shown the original tranducer response, the response of the signal sent and the signal received. The usable frequency range was 5 - 50 kHz. In Figure 2(b) is shown the time series of the received pulse.

roughness appears isotropic and stationary.

The temperature profile of the water column was measured daily with a CTD probe. The nominal water sound speed was 1525 m/s as calculated from the water temperature and salinity. The water column was isothermal within measurement error at the depths over which the experiment occurred. The site was used previously by the Generic Oceanographic Array Technologies (GOATS) experiment in 1998 [3] [4]. From this experiment, it was found that the sediment had a compressional sound speed of 1720 m/s at 200 kHz from core measurements. The attenuation was measured at 0.5 dB/m/kHz. [3]. Analysis of buried hydrophone data suggested that the sound speed at 8 kHz was 1640 m/s indicating a strong dispersion. The sediment density was measured at 1.91 g/cm^3 from cores. The shear wave speed and attenuation were not measured. From the sound speed data at the GOATS experiment, the authors predict critical angles of 28° and 22° for 200 kHz and 8 kHz respectively.

Over 256,000 measurements were collected over 5 days. Distributions of the bottom loss were determined for 20 frequency and 70 angle bins. The data appeared to be Rician distributed.

II. Data Analysis

The data were analyzed by a method similar to that reported in reference [5]. One difference in this experiment was the normalization procedure. Here, the beam pattern and experimental frequency response were measured by a calibration experiment conducted in the same general area but deeper water. For the calibration, the receiving hydrophones were pointed toward the surface creating a "virtual bottom". (See Figure 3.) Data taken in this manner allow measurement of the beam pattern of the transducers, the frequency response of the experiment and the variability due to the propagation. These calibration data were averaged and used to normalize the measured bottom loss data for spherical spreading, beam pattern and frequency response for each tranducer.

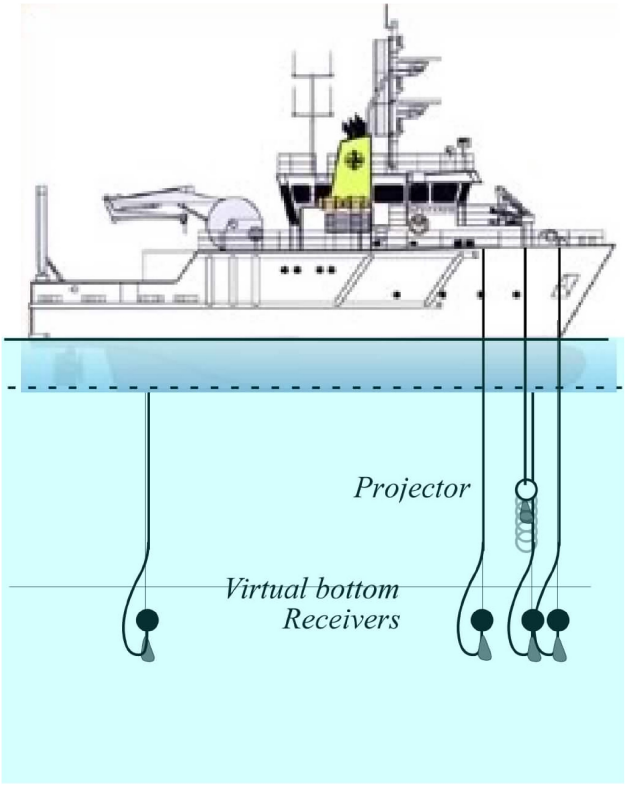

Fig. 3. Experimental Set-Up for Cailbration Measurement

III. Theory

Two theories were compared with the measurements: elastic theory in which the sediment is homogenized into an elastic solid, and the effective density fluid model [1] which includes poro-elastic effects by allowing a frequency dependent complex density. These models are summarized below and the input parameters are given.

A. Elastic Theory

Elastic theory requires five input parameters in addition to the sound speed and density of the water column. These parameters are: the compressional sound speed and attenuation, the shear sound speed and attenuation and the density.

In this case, the density, compressional sound speeds and attenuation from the GOATS(98) experiment were used. The shear wave speed and attenuation were not measured at this site. However, shear speed has been measured at 90 m/s on medium sand in a laboratory environment at 312 Hz [6]. Higher frequency measurements of shear speed are unavailable due to high attenuation. The shear attenuation can be extrapolated from measurements on unsorted sand at lower frequencies. [7]. It was found that this value has little effect on the value of the reflection coefficient. Table I summarizes the elastic model parameters.

TABLE I
ELASTIC MODEL PARAMETERS.

Parameter	Value
Sediment Density- $\mathrm{g/cm^3}$	1.91
Compressional Wave Speed - m/s	1720
Compressional Attenuation - dB/m/KHz	0.5
Shear Wave Speed - m/s	90
Shear Wave Attenuation - dB/m/KHz	0.25

B. The Effective Density Fluid Model

The effective density fluid model [1] introduces poro-elastic effects into a fluid model framework by assuming the frame bulk and shear moduli are zero. This allows the Biot equations to be simplified into fluid-like equations. The poro-elastic effects are contained in a complex, frequency dependent "effective density" and sound speed. The effective density is given by:

$$\rho_{eff} = \rho_f \frac{\alpha(1-\beta)\rho_g + \beta(\alpha-1)\rho_f + \frac{i\beta\rho F\eta}{\rho_f\omega\kappa}}{\beta(1-\beta)\rho_g + (\alpha - 2\beta + \beta^2)\rho_f + \frac{i\beta F\eta}{\omega\kappa}}, \quad (1)$$

Here, the parameter β is the porosity; α is the pore size; ρ_f is the fluid density, ρ_g is the density of the sediment grains, κ is the permeability, η is the fluid viscosity, and ω is the radial frequency. The sediment density ρ is given by $\beta\rho_f + (1-\beta)\rho_g$. F is a function derived by Biot to account for the deviation from Poisuille flow at high frequencies. [8]

The complex sound speed is represented by:

$$c = \sqrt{\frac{\left(\frac{1-\beta}{K_g} + \frac{\beta}{K_f}\right)^{-1}}{\rho_{eff}}}, \quad (2)$$

The resulting complex density from Eq. (1), compressional sound speed from Eq. (2) and attenuation which is given by the imaginary part of $\frac{\omega}{c}$ from Eq. (2) are used in the fluid model framework.

There are 9 parameters that characterize the EDFM model. These may be subdivided into two categories, bulk properties and fluid flow properties. The bulk properties are the fluid density, fluid bulk modulus, porosity, grain density and grain bulk modulus. The fluid flow properties include viscosity, permeability, tortuosity and pore size. Two bulk parameters, the fluid density and fluid bulk modulus can be assumed to be the same as the overlying water column and determined from on-site CTD measurements. The rest of the parameters are intrinsically sediment properties. Although cores were taken as part of EVA, they are not fully analyzed. Therefore, historical data must be used to provide the parameter values. One parameter, the porosity, was measured as part of the GOATS(98) experiment in the same area. [3]. Since the sand at this experiment is determined to be medium sand, the values from a similar sediment measured at the Sediment Acoustic EXperiment of 1999 (SAX99) [9] can be used. Specifically, values from SAX99 for grain density, grain bulk modulus, fluid viscosity, permeanility and tortuosity are used. The last parameter, the pore size can be calculated from the porosity, permeability and tortuosity via the Kozeny-Carmen equation. [10] Table II summarizes the values used in the models and their references.

TABLE II
PARAMETERS FOR THE EFFECTIVE DENSITY FLUID MODEL.

Parameter	Value	Reference
Fluid density- $\mathrm{g/cm^3}$	1.026	CTD Meas.
Fluid Bulk Modulus - GPa	2.40	CTD Meas.
Porosity	0.446	GOATS(98) Meas. [4]
Grain Density - $\mathrm{g/cm^3}$	2.65	SAX99 Value [11]
Grain Bulk Modulus - GPa	36	Lab. Meas.on SAX99 sand [12]
Fluid Viscosity - kg/(m s)	1.0×10^{-3}	SAX99 Value [9]
Permeability - $\mathrm{m^2}$	2.5×10^{-11}	SAX99 Meas. [13]
Tortuosity - $\mathrm{m^2}$	1.35	SAX99 Meas.. [13]
Pore Size - m	1.3×10^{-6}	Calculated [10]

C. Plane Wave Decomposition (PWD)

The source for these measurements was an ITC 1042 spherical transducer. This allowed it to be raised and lowered to probe many different grazing angles with only a small change in beam pattern. However, a spherical source can introduce spherical wave effects into the measurements especially at low frequencies. One spherical wave effect arises because sediments have an angular dependent reflection coefficient which results in a distorted semi-spherical wave reflection instead of a perfectly spherical reflection. A second effect is interference of the specular reflection and the lateral wave. The lateral wave enters the sediment at the critical angle, propagates alond the fluid/sediment interface at the speed of sound of the sediment and reradiates back into the fluid at the same critical angle. The wave attenuates with the attenuation of the sediment so at distances far from the source, the lateral wave is negligible. However, at close distances, it arrives at the same time as the specular reflection since the sediment sound speed is higher than the water sound speed. The interested reader can find color pictorials of lateral waves in Ref. [14].

Spherical wave effects can be calculated using plane wave decomposition as detailed in Ref. [15]. This method applied to a similar reflection coefficient measurement is described in Reference [5]. The difference between the PWD model for reflection coefficient and a plane wave model is shown in Figure 4. Two frequencies are shown, 5.4 kHz and 18 kHz. For the lower frequency, the spherical wave effect is evident in the decrease of the critical angle. At higher frequencies, the effect is decreased but interference with the lateral wave is still evident at sub-critical angles. The models were computed using the experimental geometry.

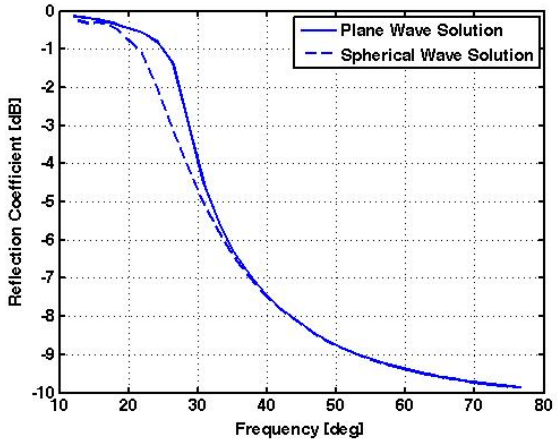

(a) Plane and Spherical Model at 5.4 kHz

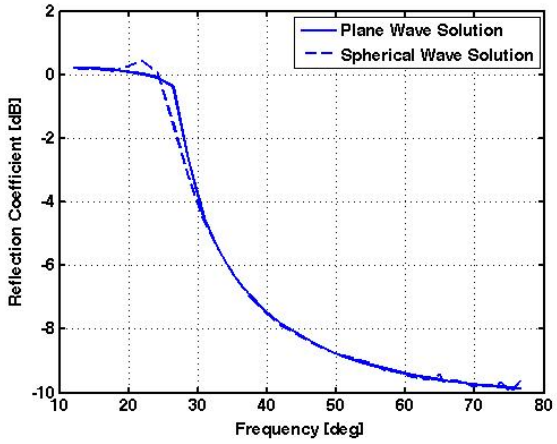

(b) Plane and Spherical Model at 18 kHz

Fig. 4. Plane and spherical wave models for 5.4 kHz, Figure 4(a) and 18 kHz, Figure 4(b). The effects are most evident at low frequencies where the spherical wave effects causes a decrease in the critical angle. However, even at higher frequencies, lateral wave interference is evident.

D. Rough Interface Scattering

The theories detailed above predict the specular reflection coefficient. In the experiment, the specular bottom loss is measured. The bottom loss measurement may be modified from the reflection coefficient by scattering from the rough sediment/water interface.

Chotiros et al in reference [16] calculated the ratio between the average amplitude in decibels of the bottom loss from the rough surface and that of an equivalent flat surface. The calculation is based on bottom roughness measurements taken on site and the experimental geometry. The correction is both angle and frequency dependent. The correction as a function of grazing angle for three frequencies is shown in Figure 5. Different angle ranges correspond to different receivers. As the scattering correction becomes large, the differences arising from the different receiver ranges become evident. These corrections are applied to the data before further analysis.

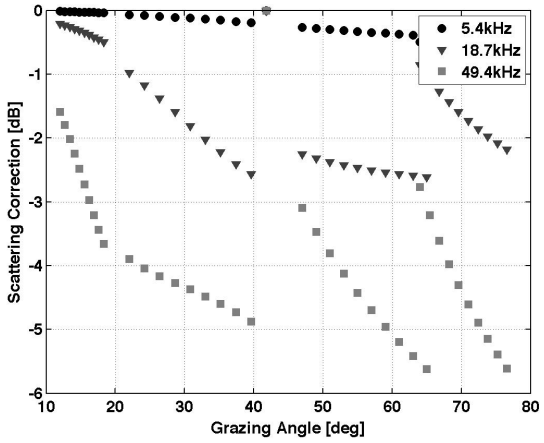

Fig. 5. Scattering correction from reference [16] to convert specular bottom loss measurements into flat interface reflection coefficients as a function of angle and frequency for the experimental geometry.

It should be noted that the scattering correction is dependent on experimental geometry and pulse length. The scattering correction shown is based on nominal values for the geometry and the pulse length as a function of frequency. Therefore, these results are considered preliminary until a more thorough analysis of the experimental pulse length may be performed.

IV. Results

The measured reflection coefficient magnitude and phase for three frequencies as a function of grazing angle are shown in Figure 6. Nineteen frequency bands were measured, but only three are shown for clarity. Also shown in the figure are the predicted values from the elastic model for each frequency corrected for spherical wave effects. The phase and magnitude of the reflection coefficient follow the expected general trend. However, to test for dispersion, the data are compared to both the elastic and EDFM model as a function of frequency for three grazing angles. The results are shown in Figure 7.

The results of the comparison of the data with the elastic model are shown in Figure 7(a). As seen in the figure, the elastic model, even including spherical wave effects, does not predict the frequency dependence of the measurements. This is especially evident in the sub-critical region and near critical. Also, there is some structure in the data at super-critical angles. This may indicate layering in the sediment.

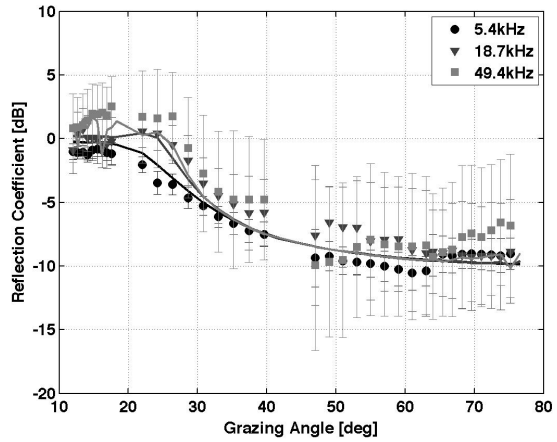

(a) Magnitude of Measured Reflection Coefficient

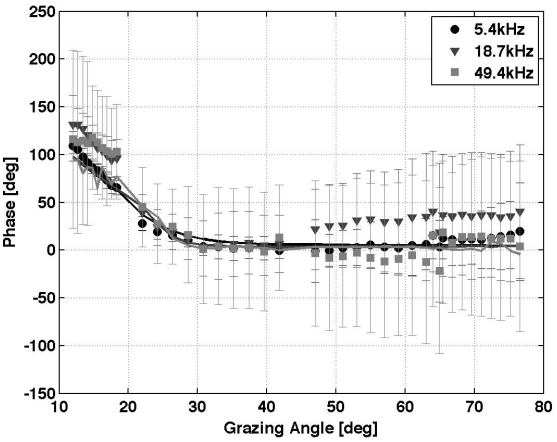

(b) Phase of Measured Reflection Coefficient

Fig. 6. Magnitude and phase of the reflection coefficient measured at EVA for three frequencies. The magnitude of the reflection coefficient has been corrected for the effects of rough surface scattering.

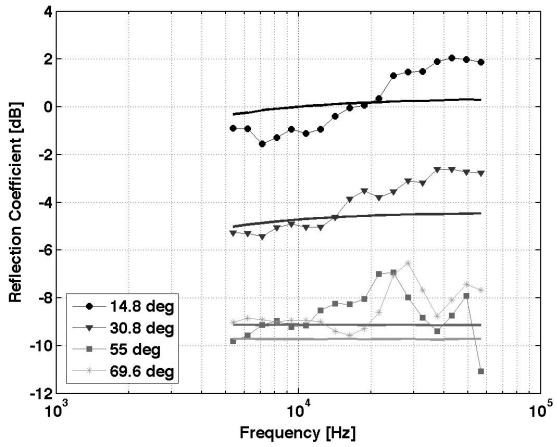

(a) Data Compared with Elastic Model

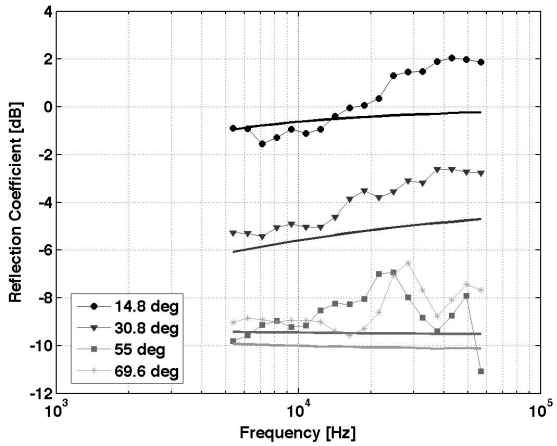

(b) Data Compared with EDFM

Fig. 7. Comparison of mean values of the measured reflection coefficient corrected for scattering with the elastic model (Figure 7(a)) and the EDFM (Figure 7(b)). The elastic model does not predict the measured dispersion in the critical angle region. The EDFM underpredicts the measurements at the critical angle.

In order to account for the measured dispersion, the measurements were compared with the EDFM in Figure 7(b). The EDFM tracks the frequency dependence of the data better, but the nominal levels are lower than predicted especially near the critical angle. Also, although the EDFM predicts more frequency dependence than the elastic model, it fails to predict the degree of frequency dependence measured in the data. At the near critical angle of 30.8 degrees, the EDFM predicts a difference in reflectivity of 1.3 dB over the frequency range, while the measured difference is almost double at 2.3 dB. In the sub-critical range, there is a also a much larger dispersion than what is predicted by the model.

Therefore, although the elastic model predicts the general trend of the magnitude of the data as a function of grazing angle, it fails to predict the measured frequency dependence, even considering spherical wave effects. The EDFM predicts more frequency dependence, but underpredicts the value of the magnitude of the reflection coefficient at sub-critical and near critical angles. Also, it predicts a much smaller degree of dispersion than measured.

The phase of the reflection coefficient follows the general trend of the predictions from the elastic model. However, a careful examination shows that the higher frequencies have higher values for phase in the sub-critical region. This may be a result of a change in the critical angle indicating dispersion. In the super-critical region, the origin of the rise in the value of the mean phase at 18.7 kHz near critical is unknown but may be due in increase in rough interface scattering at these frequencies. This causes the a high variability which may influence the mean value due to phase wrapping effects.

V. Conclusion

The magnitude and phase of the specular bottom loss was measured as a function of frequency from 5 to 50 kHz and grazing angles from 10 to 77 degrees at the Experimental Validation of Acoustic modeling techniques (EVA) sea test conducted in October 2006 in Biodola Bay, Esola d'Elba, Italy.

The measurements were normalized for spherical spreading, beam pattern and transducer response by calibration measurements taken on site. The measurements were converted to flat interface reflection coefficient values by using scattering corrections based on measurements of the seafloor roughness and experimental geometry detailed in reference [16]. These values were compared to the elastic and Effective Density Fluid Model (EDFM) [1] for both frequency and angle dependence. The models were modified to include spherical wave effects by plane wave decomposition. Parameters were determined by on-site and historical measurements. Although, the models predicted the general trend of the angle dependence of the data, they did not match the frequency dependence. The data showed a greater degree of frequency dependence at sub and near critical angles than predicted by either model. However, a further analysis of the scattering correction as a function of experimental pulse length and geometry is warranted. Furthermore, the EDFM under-predicted the values of the reflection coefficient at these angles. The super-critical angles displayed some frequency dependence which could indicate layering. Lastly, although the phase measurements follow the expected angle dependence as predicted by the elastic model on initial inspection, there was an indication of dispersion in the increase in the phase for higher frequencies in the the sub-critical region. There was also some increase in the phase at super-critical angles for mid-frequencies which may be due to an increase in the variability due to interface roughness scattering.

ACKNOWLEDGMENT

The authors thank Captain Andrea Iacono, the crew of the CRV Leonardo, Gaetano Canepa, the engineering coordinator, Per Arne Sletner and the NATO Underseas Research Center for sponsoring the ship. The authors also thank Robert Headrick and the the Office of Naval Research, Ocean Acoustics for sponsoring this work.

REFERENCES

[1] K. Williams, "An effective density fluid model for acoustic propagation in sediments derived from Biot theory," *Journal of the Acoustical Society of America*, vol. 110, pp. 2,276–2,281, 2001.

[2] N. Chotiros, M. Isakson, J. Piper, and M. Zampolli, "Seafloor roughness measurement from a ROV," in *" Proc. International Symposium on Underwater Technology 2007, 17 - 20 April, Tokyo, Japan*, 2007, pp. 52–57.

[3] A. Tesei, M. A., W. Fox, R. Lim, and H. Schmidt, "Measurements and modeling of acoustic scattering from partially and completely buried spherical shells," *Journal of the Acoustical Society of America*, vol. 112, pp. 1817–1830, 2002.

[4] M. A., W. Fox, S. H., E. Pouliquen, and B. E., "Mechanisms for subcritical penetraion into a seandy bottom: Experimental and modeling results," *Journal of the Acoustical Society of America*, vol. 107, pp. 1215–1225, 2000.

[5] H. Camin and M. Isakson, "A comparison of spherical wave sediment reflection coefficient measurements to elastic and poro-elastic models," *Journal of the Acoustical Society of America*, vol. 120, pp. 2437–2449, 2005.

[6] B. Luke, *In situ measurement of stiffness profiles in the seafloor using the spectral-analysis-of-waves (SASW) method.* Austin, TX: Technical Report under ARL:UT Independent Research and Development Program, 1995.

[7] B. Brunson, "Shear wave attenuation in unconsolidated laboratory sediments," in *Shear Waves in Marine Sediments*, J. Hovem, M. Richardson, and R. Stoll, Eds. Dordecht: Kluwer Academic Publishers., 1991, pp. 141–148.

[8] R. Stoll, "Reflection of acoustic waves at a water-sediment interface," *Journal of the Acoustical Society of America*, vol. 70, pp. 149–157, 1981.

[9] M. Richardson, K. Briggs, L. Bibee, P. Jumars, W. Sawyer, D. Albert, R. Bennett, T. Berger, M. Buckingham, N. Chotiros, P. Dahl, N. Dewitt, P. Fleischer, R. Flood, C. Greenlaw, D. Holliday, M. Hulbert, M. Hutnak, P. Jackson, J. Jaffe, H. Johnson, D. Lavoie, A. Lyons, C. Martens, D. McGehee, K. Moore, T. Orsi, J. Piper, R. Ray, A. Reed, R. Self, J. Schmidt, S. Schock, F. Simonet, R. Stoll, D. Tang, D. Thistle, E. Thorsos, D. Walter, and R. Wheatcroft, "Overview of SAX99: Environmental considerations," *IEEE Journal of Ocean Engineering*, vol. 26, pp. 26–51, 2001.

[10] P. Carmen, *Flow of Gasses through Porous Media*. New York: Academic Press, 1956.

[11] D. Tang, , K. Briggs, K. Williams, D. Jackson, E. Thorsos, and D. Percival, "Fine-scale volume heterogeneity measurements in sand," *IEEE Journal of Ocean Engineering*, vol. 27, pp. 546–560, 2002.

[12] M. Richardson, K. Williams, K. Briggs, and E. Thorsos, "Dynamic measurement of sand grain compressibility at atmospheric pressure: Acoustic applications," *IEEE Journal of Ocean Engineering*, vol. 27, pp. 593–601, 2002.

[13] K. Williams, D. Jackson, E. Thorsos, D. Tang, and S. Schock, "Comparison of sound speed and attenuation measured in a sandy sediment to predictions based on the Biot theory of porous media," *IEEE Journal of Ocean Engineering*, vol. 27, pp. 413–428, 2002.

[14] F. Jensen, W. Kuperman, P. M.B., and H. Schmidt, *Computational Ocean Acoustics*, 2nd ed. New York: Springer-Verlag, 2000.

[15] L. Brekhovskikh, *Waves in Layered Media*. New York: Academic Press, 1980.

[16] N. Chotiros, M. Isakson, J. Piper, and M. Zampolli, "Modeling of reflection coefficient fluctuation from measured seafloor roughness," in *IEEE Proceedings of the OCEANS 2007 Conference, Vancouver, B.C., Canada*, 2007.